© 2018. Published by The Company of Biologists Ltd | Journal of Cell Science (2018) 131, jcs212910. doi:10.1242/jcs.212910

SHORT REPORT

Melanopsin (Opn4) utilizes $G\alpha_i$ and $G\beta\gamma$ as major signal transducers

Dinesh Kankanamge, Kasun Ratnayake, Saroopa Samaradivakara and Ajith Karunarathne*

ABSTRACT

Melanopsin (Opn4), a ubiquitously expressed photoreceptor in all classes of vertebrates, is crucial for both visual and non-visual signaling. Opn4 supports visual functions of the eye by sensing radiance levels and discriminating contrast and brightness. Non-image-forming functions of Opn4 not only regulate circadian behavior, but also control growth and development processes of the retina. It is unclear how a single photoreceptor could govern such a diverse range of physiological functions; a role in genetic hardwiring could be one explanation, but molecular and mechanistic evidence is lacking. In addition to its role in canonical G_q pathway activation, here we demonstrate that Opn4 efficiently activates G_i heterotrimers and signals through the G protein βγ. Compared with the low levels of G_i pathway activation observed for several G_q-coupled receptors, the robust $G\alpha_i$ and $G\beta\gamma$ signaling of Opn4 led to both generation of PIP_3 and directional migration of RAW264.7 macrophages. We propose that the ability of Opn4 to signal through $G\alpha_i$ and $G\beta\gamma$ subunits is a major contributor to its functional diversity.

KEY WORDS: Melanopsin, Opn4, Retinal, GPCR, G protein, Signal transduction, Opsin

INTRODUCTION

Non-mammalian vertebrates employ Opn4, a G-protein-coupled receptor (GPCR) for extraocular photoreception (Beaulé et al., 2003). Photo-isomerization of chromophore-retinal in Opn4 induces its activation and governs downstream signaling by activating heterotrimeric G proteins. Opn4 was discovered in the melanophores of *Xenopus laevis* (African clawed frog) and later in tissues such as the eyes and deep brain of non-mammalian vertebrates (Beaulé et al., 2003; Panda et al., 2003). Two Opn4 isoforms, *Opn4L* and *Opn4S*, have been identified in mammals (Bellingham et al., 2006; Pires et al., 2007). In humans, Opn4 colocalizes with the circadian neuromodulator pituitary adenylate cyclase-activating polypeptide (ADCYAP1) in intrinsically photosensitive retinal ganglion cells (ipRGCs) (Hughes et al., 2016). They form part of the retinohypothalamic tract, which transmits photic information from the retina to suprachiasmatic nucleus to generate circadian rhythms. Opn4 is also present in other non-image-forming visual pathway structures, including the intergeniculate leaflet and olivary pretectal (Beaulé et al., 2003).

Opn4 functions as a photoreceptor by detecting brightness levels and discriminating visual signals (Brown et al., 2012). Opn4 also allows visual circuits to acquire optimal settings and perform light adaptation by measuring irradiance levels (Allen et al., 2014; Hankins and Hughes, 2014). In addition to its visual roles, Opn4 contributes to a broad range of non-visual responses, including control of the circadian clock, pupillary constriction, pineal melatonin suppression, axon regeneration after nerve system injury and sleep regulation (Li et al., 2016; Panda et al., 2003; Pilorz et al., 2016). Opn4 also influences plasma corticosterone levels, causing behavioral arousal and delaying sleep onset when exposed to blue light (Pilorz et al., 2016).

Opsins, including Opn4, belong to class A G-protein-coupled receptors (GPCRs), the largest subfamily, representing 85% of GPCR genes (Raible et al., 2006). Most opsins reported in the literature are $G_{i/o}$-coupled GPCRs (Masseck et al., 2014; Terakita, 2005), several, including Opn4, are considered G_q-coupled, whereas the only known G_s-coupled opsin to date is jellyfish opsin (Koyanagi et al., 2008). It has been suggested that Opn4 may also activate the G_i pathway (Bailes and Lucas, 2013). However, no direct evidence supports Opn4-induced Gβγ signaling. The present study shows that, in addition to its activation of the canonical G_q pathway, Opn4 also efficiently activates Gβγ signaling, which may provide a molecular explanation for its functional diversity. Gβγ controls the activity of several major signal transducers, including: (1) PI3Kγ (Kolsch et al., 2008), (2) adenylyl cyclase (AC) isoforms (activation of AC2, AC4 and AC7; inhibition of AC1 and AC5) (Sunahara and Taussig, 2002; Tang and Gilman, 1991), (3) inwardly rectifying potassium channels (Kawano et al., 1999; Nakajima et al., 1996), (4) PLC isoforms ($PLC\beta_2$, $PLC\beta_3$) (Camps et al., 1992; Smrcka and Sternweis, 1993), (5) Ca^{2+} channels (N, P/Q type) (Herlitze et al., 1996; Ikeda, 1996), (6) GPCR kinase 2 (Pitcher et al., 1992), and (7) GEFs, including Rac, Cdc42 GEF (FLJ00018) and p114-GEF (Mayeenuddin et al., 2006; Niu et al., 2003; Ueda et al., 2008). The ability of Gβγ to control such a large number of signaling regulators should allow cells to utilize Gβγ signaling via Opn4 to perform their designated functions.

RESULTS AND DISCUSSION

Activated Opn4, but not ligand-binding G_q-coupled GPCRs, efficiently induces Gβγ translocation

Our goal was to show that Opn4 possesses distinct heterotrimer activation abilities compared with other G_q-coupled GPCRs. $G\alpha_q$GTP generated upon G_q-coupled GPCR (including Opn4) activation stimulates PLCβ, which hydrolyzes the plasma membrane (PM) phospholipid, PIP_2, and generates IP_3 and DAG. HeLa cells expressing Opn4, mCherry-γ_9 and Venus-PH exhibited robust translocation of mCherry-γ_9 from the PM to inner membranes (IMs), with simultaneous PIP_2 hydrolysis (Fig. 1A, left, Movies 1 and 2) when Opn4 is photoactivated at 515 nm in the presence of 50 µM 11-*cis*-retinal. Mean fluorescence changes in IMs (white arrow) and cytosol represent the rate and extent of $G\gamma_9$ translocation and PIP_2 hydrolysis, respectively. Despite its

Department of Chemistry and Biochemistry, The University of Toledo, Toledo, OH 43606, USA.

*Author for correspondence (Ajith.karunarathne@utoledo.edu)

A.K., 0000-0003-3136-2015

Received 7 November 2017; Accepted 23 April 2018

Journal of Cell Science (2018) 131, jcs212910. doi:10.1242/jcs.212910

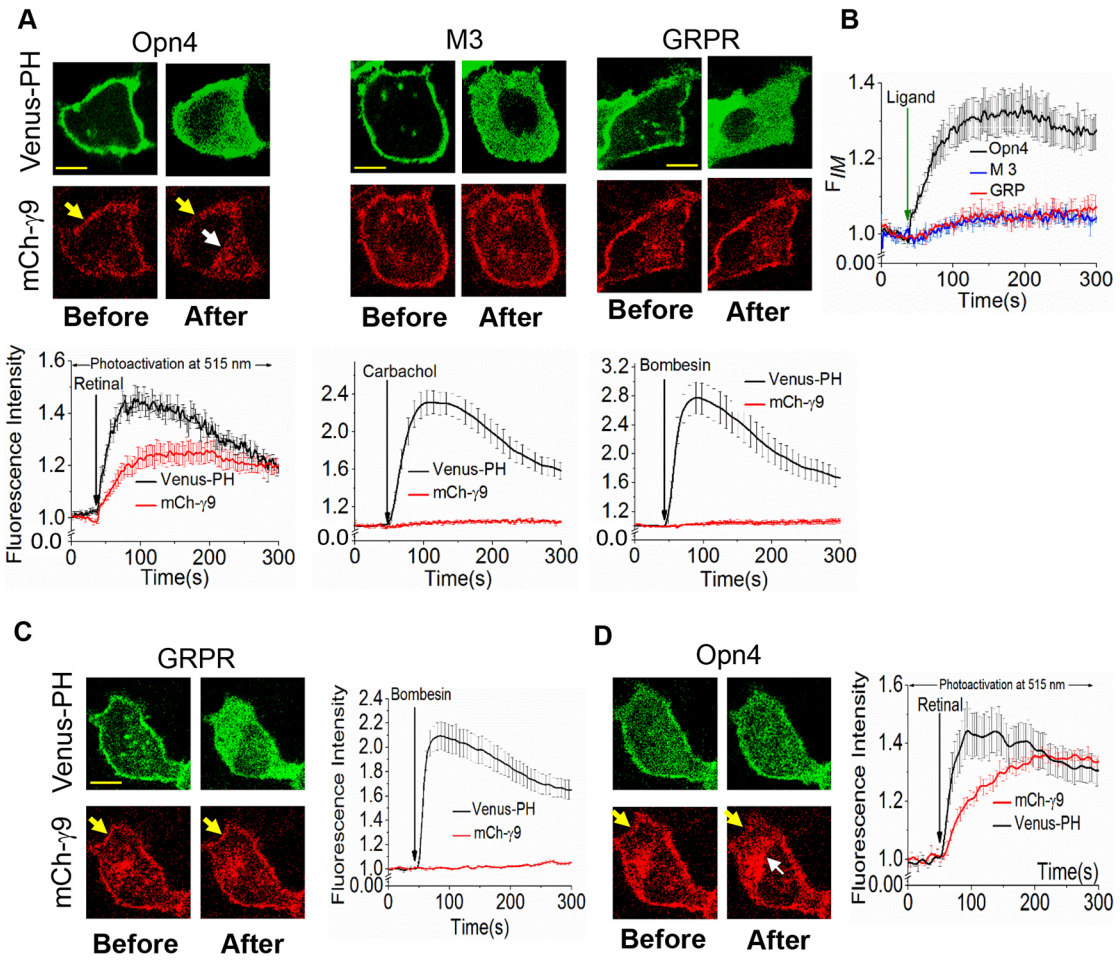

Fig. 1. Ligand binding G_q-coupled GPCRs show only G_q pathway activation while Opn4 additionally induces Gβγ translocation. PIP_2 hydrolysis, and mCherry-$G\gamma_9$ and Venus-PH translocation in HeLa cells transiently expressing Opn4, GRPR and M3. (A) Opn4 activation by adding retinal at 50 s while exposing cells to 515 nm light (Venus-PH), induced mCherry-γ_9 translocation and PIP_2 hydrolysis. Activated GRPR and M3 exhibited PIP_2 hydrolysis but lacked pronounced $G\gamma_9$ translocation. (B) Relative mCherry-γ_9 translocation induced by activated Opn4, M3 and GRP receptors. (C) The same cells expressing Opn4, GRPR, mCherry-γ_9 and Venus-PH were first activated with 1 µM bombesin at 50 s. Cells show PIP_2 hydrolysis but lack $G\gamma_9$ translocation. (D) After PIP_2 recovery at the PM, 11-*cis*-retinal (50 µM) was added to the cell shown in C. The cell exhibited PIP_2 hydrolysis and robust $G\gamma_9$ translocation from the PM (yellow arrows) to IMs (white arrows). Scale bars: 10 µm. Average curves are shown for $n \geq 10$ cells from ≥3 independent experiments. Results are mean±s.e.m.

previously shown promiscuity towards G_i heterotrimers (Offermanns et al., 1994; van Unen et al., 2016), G_q-coupled M3-muscarinic receptor (M3R) activation in HeLa cells only exhibited minor translocation of mCherry-γ_9 (Fig. 1A, middle, Movie 3). The G_q-coupled gastrin-releasing peptide receptor (GRPR) responded similarly (Movie 4). Nevertheless, Opn4, M3R and GRPR activation exhibited comparable PIP_2 hydrolysis responses (Fig. 1A). These data indicate that, like G_i-coupled GPCRs, Opn4 is more efficient at translocating free Gβγ than both M3R and GRPR (Fig. 1B); however, different expression levels of receptors could alter the extent of signaling. Control cells lacking receptor expression did not exhibit PIP_2 hydrolysis upon exposure to carbachol, bombesin or 515 nm light (Fig. S1A), thus the Gβγ translocation observed is a result of αGTP and free Gβγ generated by activated GPCRs (Akgoz et al., 2004, 2006; Bondar and Lazar, 2014).

We compared activated Opn4, G_i-coupled α2-AR and CXCR4-induced Gβγ translocations (Movie 5). The broad absorption spectrum of Opn4 (λ_{max}~480 nm) (Enezi et al., 2011; van Oosterhout et al., 2012), allowed imaging of the fluorescence sensor upon photoactivation at 445, 488 and 515 nm (Fig. S1B). Activated Opn4, α_2AR and CXCR4 exhibited comparable $G\gamma_9$ translocations (Fig. S2). To demonstrate the distinct ability of Opn4 to induce Gβγ translocation compared with G_q-coupled GRPR, sequential activation of these receptors was examined in the same cells. HeLa cells expressing both Opn4 and GRPR together with mCherry-γ_9 and Venus-PH were imaged using 515 nm and 595 nm excitation wavelengths. At 40 s, GRPRs were activated using 1 µM bombesin (Fig. 1C). Although an intense PIP_2 hydrolysis and robust recovery were observed, mCherry-γ_9 translocation was not detected (Fig. 1C, graph). After PIP_2 recovery, adding 11-*cis*-retinal at 50 s activated Opn4 in the same cell. Both PIP_2 hydrolysis and robust mCherry-γ_9 translocation were observed (Fig. 1D). This demonstrates the ability of activated Opn4, like α2-AR and CXCR4, to efficiently generate Gβγ (Senarath et al., 2016).

Opn4 activation generates free Gβγ, primarily through activation of $G_{i/o}$ heterotrimers

Our next goal was to decipher the origin of free Gβγ generated by activated Opn4. $G\beta\gamma_9$ translocation and PIP_2 hydrolysis were examined in the presence of pertussis toxin (PTx). PTx catalyzes ADP-ribosylation of the $G\alpha_i$ subunit and prevents coupling of

Journal of Cell Science (2018) 131, jcs212910. doi:10.1242/jcs.212910

heterotrimers to GPCR (Ribeiro-Neto and Rodbell, 1989). HeLa cells expressing Opn4, mCherry-γ_9 and YFP-PH were incubated with 100 nM PTx for 5 h at 37°C. Opn4 activation did not induce G$\beta\gamma_9$ translocation (Fig. 2A, top). Interestingly, the same cells exhibited PIP_2 hydrolysis (Fig. 2A, bottom). This demonstrates that Opn4 induces translocation of G$\beta\gamma_9$ generated through the G_i pathway. Whether the observed G$\beta\gamma$ translocation is a result of G_q heterotrimer activation was examined. HeLa cells were incubated with G_q inhibitor YM-254890 (1 µM) for 5 min at 37°C, to block G_q heterotrimer dissociation by preventing GDP-GTP exchange (Takasaki et al., 2004). With YM-254890, Opn4 activation still induced efficient G$\beta\gamma_9$ translocation (Fig. 2B, top) from the PM (yellow arrows) to IMs (white arrow), while G_q-mediated PIP_2 hydrolysis was abolished (Fig. 2B, bottom). Similarly, HeLa cells treated with only vehicle solvent used for PTx (Fig. S3A) and YM-254890 (Fig. S3B) exhibited both PIP_2 hydrolysis and Gγ_9 translocation. Collectively, these data suggest that Opn4 can simultaneously activate Gα_i and Gα_q signaling in the same cells to a comparable extent, and Gα_i-heterotrimer activation induces G$\beta\gamma$ translocation. Whether Opn4 activates translocation of other Gγ subunits was also examined. HeLa cells transiently expressing Opn4 and either YFP-γ_1 or YFP-γ_{11} and pre-treated with 11-*cis*-retinal exhibited significant Gγ_1 and Gγ_{11} translocations from the PM (yellow arrows) to IMs (white arrows) upon Opn4 activation (Fig. 2C). Similarly, Opn4 activation also induced Gβ_1-YFP translocation (Fig. 2C, bottom). This clearly demonstrates that Opn4 activates G protein heterotrimers, regardless of Gγ subtype. Gβ_1 translocation indicates that it translocates as a G$\beta\gamma$ dimer, as we have showed previously (Senarath et al., 2018).

Dimerization of certain GPCR combinations, activating distinct heterotrimer types has been demonstrated (Terrillon and Bouvier, 2004). To test the likelihood of Opn4 forming a heterodimer with a specific G_i-coupled GPCR in HeLa cells, activation of G_i signaling upon optical activation of Opn4 was examined using H125 lung carcinoma cells. The different origins of HeLa and H125 cells makes it highly unlikely that both cell types express the same GPCR, which can dimerize with Opn4 to induce its G_i activity. H125 cells expressing Opn4, mCherry-γ_9 and Venus-PH, pre-incubated with 11-*cis*-retinal, also exhibited both mCherry-γ_9 translocation (yellow and white arrows) and PIP_2 hydrolysis upon Opn4 activation (Fig. 2D). This indicates that Opn4 induces mCherry-γ_9 translocation.

Opn4 induces downstream signaling through Gα_q, Gα_i and G$\beta\gamma$

The next objective was to examine concurrent activation of Gα_q and G$\beta\gamma$ effectors by activated Opn4. Both GαqGTP and G$\beta\gamma$ activate PLCβ, hydrolyzing PIP_2 to IP_3 and DAG (Park et al., 1993; Wu et al., 1993). DAG stays bound to the PM (Kamp and Hell, 2000; Park et al., 1993). Generation of DAG in HeLa cells was measured using translocation of an mCherry-conjugated DAG binding domain (DBD) sensor from the cytosol to the PM (Gallegos et al., 2006). 11-*cis*-retinal was added at 50 s to HeLa cells expressing mCherry-DBD and Opn4-YFP. Upon Opn4 activation, cytosolic DAG sensor translocated to the PM (Fig. 3A, top). While the receptor remained in an active state, the DBD sensor reverse-translocated to the cytosol, probably due to adaptation of PIP_2 hydrolysis (Ferguson and Caron, 1998; Gainetdinov et al., 2004). Cells treated with G_q inhibitor did not exhibit any detectable mCherry-DBD translocation (Fig. 3A, bottom). Calcium mobilization elicited by Opn4-generated IP_3 was measured using HeLa cells pre-incubated with the calcium indicator Fluo-4 AM

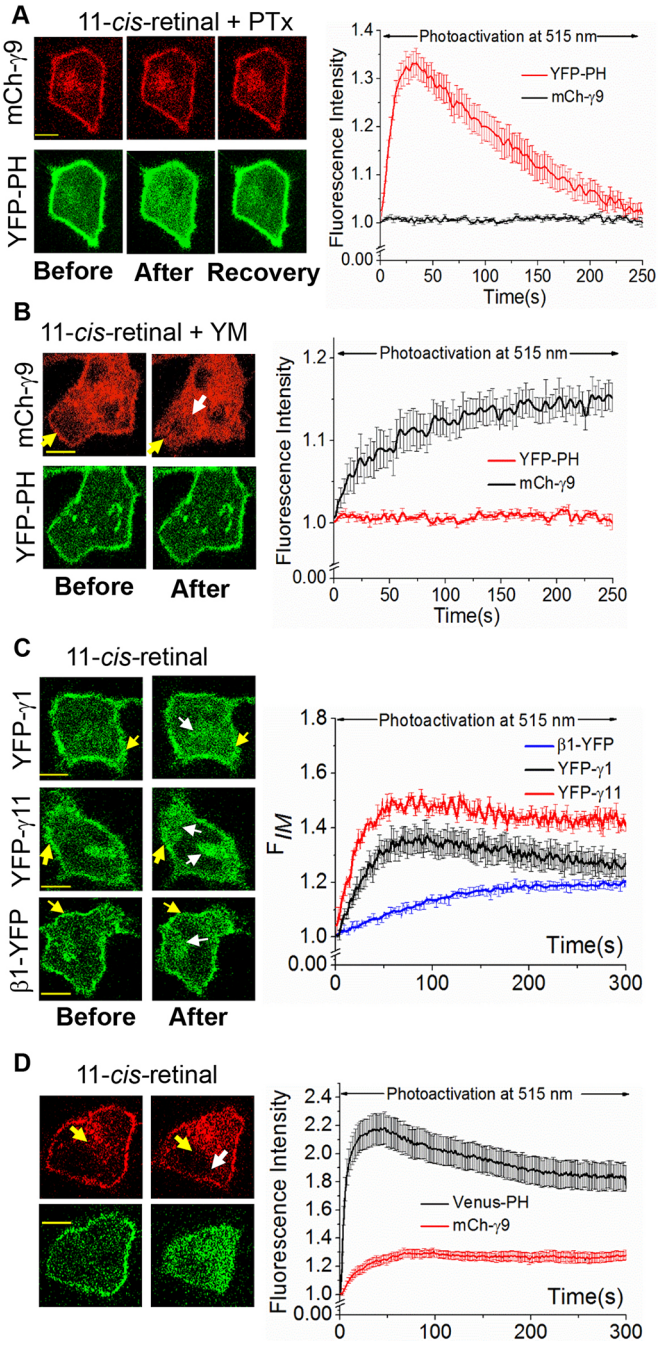

Fig. 2. Opn4 exhibits concurrent activation of both G_i and G_q heterotrimers. PIP_2 hydrolysis (YFP-PH) and Gγ_9 translocation (mCherry-Gγ_9) in HeLa cells (pre-incubated with 50 µM 11-*cis*-retinal) after activation of Opn4 in the presence of (A) PTx (100 nM) and (B) G_q inhibitor YM-254890 (1 µM). PTx inhibited Gγ_9 translocation, YM-254890 inhibited PIP_2 hydrolysis. (C) Opn4 activation induced translocation of YFP tagged γ_1 (top), γ_{11} (middle) and β_1 (bottom) in HeLa cells pre-incubated with 50 µM 11-*cis*-retinal. (D) PIP_2 hydrolysis, γ_9 translocation upon Opn4 activation in H125 cells. Yellow arrows, PM; white arrows, IM. Scale bars: 10 µm. Average curves are plotted for $n \geq 10$ cells from ≥3 independent experiments. Results are mean±s.e.m.

(2.28 µM). Cells were imaged using 488 nm excitation and 515 nm emission to capture Fluo-4 fluorescence. Opn4-expressing cells exhibited increases in Ca^{2+} upon addition of 11-*cis*-retinal, which was transient and gradually disappeared (Fig. 3B, top). Cells incubated with G_q inhibitor did not exhibit any Ca^{2+} increase on Opn4 activation (Fig. 3B, bottom). These data suggest that

Journal of Cell Science (2018) 131, jcs212910. doi:10.1242/jcs.212910

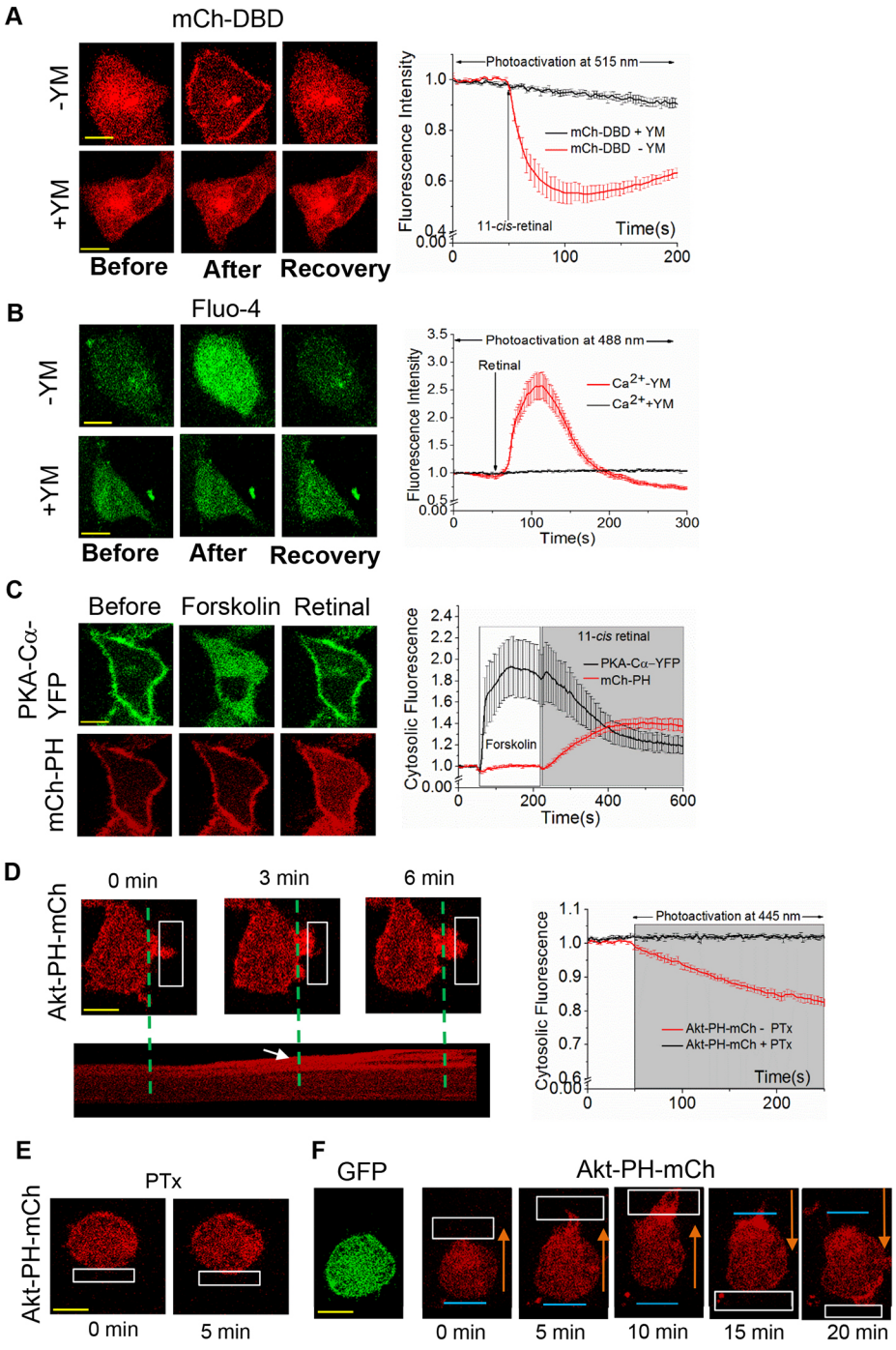

Fig. 3. Opn4 activates PLCβ, AC and PI3K signaling through $G\alpha_q$, $G\alpha_i$ and $G\beta\gamma$, respectively. (A) DAG formation on PM in HeLa cells with and without the G_q inhibitor (YM-254890) after Opn4 activation. YM-254890 inhibited DAG formation. (B) Opn4 induced cytosolic Ca^{2+} responses in HeLa cells with and without G_q inhibitor. YM-254890 inhibited the Ca^{2+} response. (C) Opn4-induced $G\alpha_i$ activation inhibited the forskolin-IBMX induced AC activation and cAMP generation (PKA-δRIIβ: PKA-Cα-YFP). PIP_3 production in RAW264.7 cells (pre-incubated with 50 µM 11-*cis*-retinal) upon optical activation of Opn4 in the absence (D) and presence of 100 ng/ml PTx (E). (F) Time-lapse images show Opn4-induced PIP_3 production at the leading edge of RAW264.7 cells and directional migration (orange arrows) in the presence of G_q inhibitor (blue line indicates start). Scale bars: 10 µm. Average curves plotted for n=10 cells from ≥3 independent experiments. Results are mean±s.e.m.

G_q-pathway activation is primarily responsible for Opn4-regulated Ca^{2+} and DAG signaling. G_i pathway activation by Opn4 was measured in HeLa cells using a bi-molecular translocation-based cAMP sensor, PKA-δRIIβ: PKA-Cα-YFP (Dyachok et al., 2006; Siripurapu et al., 2017). Briefly, HeLa cells expressing Opn4, cAMP sensor, and mCherry-PH were exposed to 10 µM forskolin in IBMX (3-isobutyl-1-methylxanthine). Cells exhibited complete translocation of PKA-Cα-YFP from the PM to the cytosol, indicating cAMP generation (Fig. 3C, top middle). After ∼3 min, 11-*cis*-retinal was added, activating Opn4, and cells exhibited a reverse translocation of PKA-Cα-YFP. This indicates $G\alpha_i$-mediated inhibition of AC and cAMP production. A simultaneous PIP_2 hydrolysis upon Opn4 activation was also observed (Fig. 3C, bottom).

Gβγ is a crucial signal transducer for cellular homeostasis and it controls a cohort of essential effectors in the GPCR pathway. We demonstrated that only cells expressing high PM affinity Gγ subtypes (γ_2, γ_3) activate PM-bound effectors of Gβγ, including PI3K and PLBβ (Senarath et al., 2018). HeLa cells lack γ_2 and γ_3, and exhibit only minor PIP_3 production upon G_i pathway activation, whereas γ_3-expressing RAW264.7 cells exhibit PIP_3 production (Senarath et al., 2018). We also showed that localized G_i pathway activation and Gβγ generation in RAW264.7 cells induces directional migration, accompanied by PIP_3 generation at the leading edge (Senarath et al., 2018; Siripurapu et al., 2017). Thus, Opn4-induced PIP_3 generation and cell migration were examined using RAW264.7 cells. RAW264.7 cells expressing Opn4-GFP and

Journal of Cell Science (2018) 131, jcs212910. doi:10.1242/jcs.212910

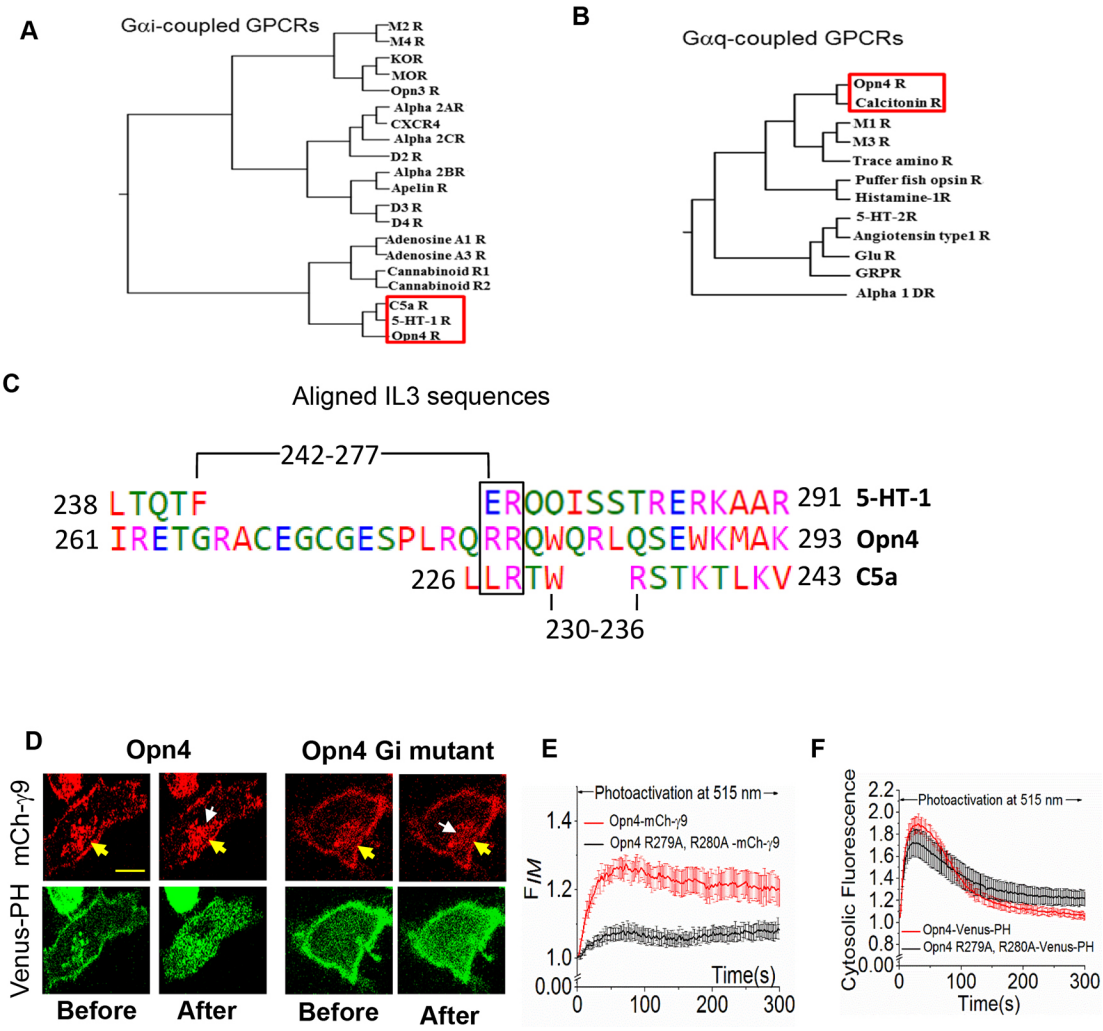

Fig. 4. Opn4 sequence and its dual pathway (G_i, G_q) activation ability. (A) Phylogenetic analysis of G_i-coupled GPCRs based on sequence alignment for IL3 regions. C5a and 5-HT-1 clustered with Opn4 (red box). (B) G_q-coupled GPCR, calcitonin clusters with Opn4 based on IL3-regions (red box). (C) Sequence alignments for G_i-coupled 5HT-1-Opn4 and C5a-Opn4. The mutations in box (R to A) resulted in a G_i-activity deficient mutant. (D) $G\gamma_9$ translocation and PIP_2 hydrolysis after activating wild-type Opn4 (left) and a G_i-deficient mutant of Opn4 (right). Yellow arrows, PM; white arrows, IM. (E) $G\gamma_9$ translocation induced by a G_i-deficient mutant of Opn4 is minor compared with that induced by wild-type Opn4. Difference in the extent of γ_9 translocation exhibited by wild-type and mutant Opn4 is statistically significant (P<0.0001). (F) WT and mutant Opn4 induce similar levels of PIP_2 hydrolysis. Scale bar: 10 µm. Average curves plotted for $n \geq 10$ cells from ≥3 independent experiments. Results are mean±s.e.m.

Akt-PH-mCherry (PIP_3 sensor) and treated with 11-*cis*-retinal were exposed to a spatially restricted blue light stimulus (Fig. 3D, white box). Time-lapse images clearly indicate PIP_3 production at the optically activated leading edge. The orthogonal slice shows accumulation of PIP_3 at the PM (white arrow) (Fig. 3D). This Opn4-induced PIP_3 production was abolished by PTx (Fig. 3E), as well as by the Gβγ inhibitor Gallein (Lehmann et al., 2008) (Fig. S3C). This indicates that Opn4-induced PIP_3 production is independent of the G_q pathway and is governed by free Gβγ. Additionally, activation of Opn4 in the presence of G_q inhibitor resulted in not only PIP_3 production but also a noticeable cell migration (Fig. 3F). Generated PIP_3 alone can activate many signaling pathways, including Akt/PKB, several GEFs (Tiam1, P-Rex1), tyrosine kinase (Btk), and growth factor receptor-bound protein 2 (Grb2) to control cellular functions ranging from migration to gene transcription (Chen et al., 2012; Karunarathne et al., 2013; Weiner, 2002). Since Opn4 induces PIP_3 generation, in addition to its signaling through $G\alpha_i$, it should control PIP_3-regulated pathways, thus affecting diverse cellular functions.

Sequence properties of Opn4 that enable its ability to activate both G_i and G_q pathways

Since Opn4 short (Opn4S) and long (Opn4L) splice variants in ipRGCs are anticipated to deliver diverse cellular functions (Hughes et al., 2012; Pires et al., 2009), we examined whether they possess distinct signaling activities. We generated Opn4S by truncating the C-terminus (Ct) of Opn4L (or Opn4). When expressed in HeLa cells, Opn4S and Opn4L exhibited similar signaling properties (Fig. 1A, left, Fig. S4A). Overall, these data suggest that G_i and G_q pathway selectivity in Opn4 is independent of its Ct domain.

To govern both G_i and G_q signaling, Opn4 should be able to interact with both G_i and G_q heterotrimers. GPCRs recognize heterotrimers with appropriate Gα types, primarily using intracellular loop 3 (IL3) (Itoh et al., 2001). We examined IL3 regions of G_i- and G_q-coupled GPCRs and compared them with the IL3 sequence of Opn4 using MAFFT multiple sequence alignment software (Fig. 4A,B) (Katoh et al., 2002; Katoh and Standley, 2013). This analysis showed that IL3 of Opn4 clustered with the IL3 regions of G_i-coupled complement 5a receptor (C5a) and serotonin receptor

(5-HT-1) (Fig. 4A), and the IL3 region of Opn4 clustered with G_q-coupled calcitonin receptor (Fig. 4B). Interestingly, the left side of the IL3 region of Opn4 exhibited G_q-coupled (Fig. S4B) whereas the right side showed G_i-coupled GPCR-like characteristics (Fig. 4C). Left side mutations of IL3 – R262A, E263A and T264A (Fig. S4B, box) – resulted in completely non-responsive Opn4. This result suggests either that G_q-Opn4 coupling prior to G_i heterotrimer formation is crucial for their activation, or that mutations in the left side of IL3 may alter Opn4 conformation, rendering it non-functional. Among right side mutations, mutant R279A, R280A Opn4 (Fig. 4C, box) exhibited a 4-fold lower level of mCherry-γ_9 translocation compared with wild-type Opn4 (Fig. 4D,E). Its ability to induce PIP_2 hydrolysis remained intact (Fig. 4D,F). This further suggests that Opn4 interacts with and activates both G_q and G_i heterotrimers.

Since Opn4 can activate $G\alpha_i$ and regulate cAMP, it can control axonal regeneration and sleep regulation (Hannila and Filbin, 2008; Spencer and Filbin, 2004). G_i-coupled melatonin 2 receptor controls circadian rhythms by regulating both $G\alpha_i$ and $G\beta\gamma$ (Dubocovich and Markowska, 2005; Dubocovich et al., 2003). Muscarinic receptor-induced G_i signaling has been shown to regulate pupillary constriction and dilation in human (Abrams et al., 2006), serum corticosterone levels and the sleep-wake cycle in mice (Hemrick-Luecke et al., 2002). Therefore, Opn4 can regulate these functions by activating G_i pathway. Considering the broad range of effectors and cellular functions controlled by the G_i pathway, especially through $G\beta\gamma$, the functional diversity of Opn4 and its ability to signal through multiple pathways are likely to be linked.

MATERIALS AND METHODS

DNA constructs, reagents and cell lines

YFP-PH cDNA has been previously described (Gallegos et al., 2006). Bi-cistronic Opn4-GFP, mCherry-γ_9, mCherry-PH, M3R, mCherry-DBD, Venus-PH and Akt-PH-mCherry cDNAs were kindly provided by Professor Narasimhan Gautam's lab (Washington University, St Louis, MO). GRPR was a kind gift from the lab of Zhou-Feng Chen (Washington University, St Louis, MO). Opn4 PCR product was inserted into *Kpn*I and *Xba*I sites in pcDNA 3.1 to create untagged Opn4. Opn4S was created by adding a stop codon to Opn4L after aligning splice variants (Opn4L and Opn4S). Overlap PCR and Gibson assembly were performed to generate Opn4 R279A, R280A mutant based on multiple sequence alignment data described. Reagent sources are as follows: pertussis toxin (PTx) and norepinephrine (Sigma-Aldrich), Gibson assembly master mix and competent cells (NEB, Ipswich, MA, USA), YM-254890 (Focus Biomolecules, Plymouth Meeting, PA, USA), Fluo-4 AM (Molecular Probes, Eugene, OR, USA), Bombesin (Tocris, Park Ellisville, MO, USA), Carbachol (Fisher Scientific, Pittsburgh, PA, USA), SDF-1α (PeproTech, Rocky Hill, NJ, USA), 11-*cis*-retinal (National Eye Institute, Bethesda, MD, USA), PolyJet (SignaGen, Rockville, MD, USA), IBMX and Forskolin (Cayman Chemical, Ann Arbor, MI, USA). All the reagents were dissolved in the appropriate solvent according to the manufacturers' instructions and diluted in 1% HBSS supplemented with $NaHCO_3$ or regular cell culture medium before adding to cells. Cell lines (HeLa, RAW264.7) were originally purchased from the American Tissue Culture Collection (ATCC, Manassas, VA, USA) and authenticated using a commercial kit to amplify 9 unique STR loci. NCI-H125 cell line was kindly provided by Dr Randall Ruch (University of Toledo, OH, USA).

Cell culture and transfections

RAW264.7 mouse macrophage cell line (ATCC) was cultured in RPMI 1640 (10-041-CV; CORNING, Manassas, VA, USA) with 10% fetal bovine serum (Atlanta Biologicals, Flowery Branch, GA, USA), L-glutamine and 1% penicillin-streptomycin in a humidified incubator at 37°C and 5% CO_2. At 75% confluency, cells were lifted after incubation with versene-EDTA (CellGro) for 3 min at 37°C, centrifuged at 1000 ***g*** for 3 min and versene-EDTA was aspirated before resuspending cells in RPMI 1640 with 10% dialyzed fetal bovine serum at 8×10^4/ml cell density. One day before transfection of DNA into cells, 8×10^4 cells were seeded on 35 mm glass bottom dishes (In Vitro Scientific). HeLa cells (ATCC) were cultured in minimum essential medium (CellGro) containing 10% fetal bovine serum (Atlanta Biologicals), in the presence of 1% penicillin-streptomycin in 60 mm tissue culture dishes in a humidified incubator at 37°C, 5% CO_2. The remaining cell culture procedures for HeLa cells were similar to the protocols described above for RAW264.7 cells. Transfection was performed using PolyJet transfection reagent (SignaGen, Rockville, MD, USA) according to the manufacturer's protocol and imaging was performed 12-14 h after transfection. Before imaging, cell culture medium was replaced with Hank's Balanced Salt Solution (HBSS) that was equilibrated for 1 h at 37°C and 5% CO_2.

Phylogenetic analysis

G_i- and G_q-coupled GPCRs were identified (Alexander et al., 1999, 2017). The IL3 regions of G_i- and G_q-coupled receptors were examined by HMMTOP transmembrane prediction software (http://www.enzim.hu/hmmtop/). GenomeNet bioinformatics tools (http://www.genome.jp/en/gn_tools.html) were utilized to perform sequence analysis and tree generation. Sequences of IL3 regions of G_i- and G_q-coupled receptors were aligned using MAFFT (Katoh and Standley, 2013; https://mafft.cbrc.jp/alignment/software/). Aligned sequence phylogenies were subjected to unweighted pair-group method using arithmetic averages (UPGMA) clustering to generate phylogenetic trees.

Opn4 activation and imaging of PIP_2 hydrolysis, DAG formation, PIP3 and cAMP production, and $G\beta\gamma$ translocation

A Nikon-Andor spinning disk confocal imaging system, with a Nikon Ti-R/B inverted microscope, a Yokogawa CSU-X1 spinning disk unit (5000 rpm) and iXon ULTRA 897BV back illuminated deep-cooled EMCCD camera was used. Photo-activation of selected regions of Opn4 was conducted using an Andor Fluorescence Recovery After Photo bleach and Photo Activation (FRAP-PA) unit. All DNA constructs were transiently transfected and cells were imaged after overnight transfection. Bi-cistronic vectors carrying Opn4 and GFP, Opn4 untagged and Opn-4GFP constructs were used to transiently express Opn4 and their expression was confirmed by using cytosolic GFP, PIP_2 hydrolysis or $G\beta\gamma$ translocation on activation or using the GFP tag, respectively. Imaging of cells was carried out using a 60×, 1.4 NA oil objective employing 50 mW 445, 488, 515, 595 nm solid-state lasers. Sensors were imaged using the following settings: GFP and Fluo-4 AM, 488 nm at 56 µW/515 nm; YFP and Venus, 515 nm at 22 µW/540 nm; mCherry, 594 nm at 20 µW/630 nm (excitation/emission). Cells were pre-incubated with 50 µM 11-*cis*-retinal unless otherwise specified. Optical activation was performed using a FRAP-PA device by drawing a desired light exposure region in the field of vision and exposing those areas to 445 nm blue light pulsed at 1 Hz at 0.22 µW. Imaging of sensors for PIP_2, PIP_3, DAG and $G\gamma_9$ translocation were also performed at 1 Hz; since Opn4 has a broad absorption spectra, imaging YFP activates it. Digital image analysis was performed using Andor iQ 3.1 software and fluorescence intensity obtained from regions of interest (PM, IMs and cytosol) was normalized to initial value (baseline). Normalized data were then plotted using Origin pro (OriginLab Corporation). Results of all quantitative assays ($G\beta\gamma$ translocation and PIP_2 hydrolysis, Ca^{2+} responses) are expressed as standard error of mean (s.e.m.) from *n* number of cells (indicated in the figure legends) on multiple days, using cells with a different passage number.

Intracellular Ca^{2+} measurements

For cytosolic Ca^{2+} measurements, HeLa cells were cultured on glass-bottomed dishes in MEM/DFBS at 37°C with 5% CO_2 as described above. Experiments were performed 12-24 h after transfection of DNA. Opn4-transfected cells were washed twice with 1% (v/v) HBSS supplemented with $NaHCO_3$ and Ca^{2+}, adjusted to pH 7.2, and incubated for 30 min at room temperature with the fluorescent Ca^{2+} indicator, Fluo-4 AM (2.28 µM) in dark conditions. Before imaging, cells were again washed twice with 1% HBSS supplemented with $NaHCO_3$ and Ca^{2+} to remove excess Fluo-4 AM.

Processed dishes were mounted and fluorescence intensity of Fluo-4 AM (488 nm) was continuously imaged at 1 s intervals using 488 nm excitation, 515 nm emission for confocal microscopy. Fluo-4 AM fluorescence intensity obtained from regions of interest was normalized to initial value.

Statistics and reproducibility

Results of all quantitative assays (PIP_2 hydrolysis, PIP_3 generation, Gγ translocation, DAG formation, calcium, cAMP production) were computed as mean±s.e.m. from ≥10 cells in multiple independent experiments (>3) unless otherwise specified. Statistical analysis of the extent of Gγ9 translocation induced by wild-type and mutant Opn4 was performed using two-tailed unpaired *t*-test. The two means were significantly different at $P<0.0001$.

Acknowledgements

We thank Prof. Narasimhan Gautam for cDNA for G proteins, GPCRs and sensors; Dr Matthew Toomey for R script generating opsin spectra; Dr Anders Tengholm for providing bi-molecular cAMP probe; Dr John L. Payton, Mithila Tennakoon, Kanishka Senarath and Zehra Fasih for experimental assistance, discussions and comments. We acknowledge the National Eye Institute for providing 11-*cis*-retinal.

Competing interests

The authors declare no competing or financial interests.

Author contributions

Conceptualization: D.K., A.K.; Methodology: D.K., K.R., A.K.; Software: D.K., A.K.; Validation: D.K., K.R., A.K.; Formal analysis: D.K., K.R., A.K.; Investigation: D.K., K.R., S.S., A.K.; Resources: A.K.; Writing - original draft: D.K., K.R., S.S., A.K.; Writing - review & editing: D.K., K.R., A.K.; Visualization: D.K., A.K.; Supervision: A.K.; Project administration: A.K.; Funding acquisition: A.K.

Funding

This work was funded by the University of Toledo.

Supplementary information

Supplementary information available online at
http://jcs.biologists.org/lookup/doi/10.1242/jcs.212910.supplemental

References

Abrams, P., Andersson, K.-E., Buccafusco, J. J., Chapple, C., de Groat, W. C., Fryer, A. D., Kay, G., Laties, A., Nathanson, N. M., Pasricha, P. J. et al. (2006). Muscarinic receptors: their distribution and function in body systems, and the implications for treating overactive bladder. *Br. J. Pharmacol.* **148**, 565-578.

Akgoz, M., Kalyanaraman, V. and Gautam, N. (2004). Receptor-mediated reversible translocation of the G protein betagamma complex from the plasma membrane to the Golgi complex. *J. Biol. Chem.* **279**, 51541-51544.

Akgoz, M., Kalyanaraman, V. and Gautam, N. (2006). G protein betagamma complex translocation from plasma membrane to Golgi complex is influenced by receptor gamma subunit interaction. *Cell. Signal.* **18**, 1758-1768.

Alexander, S., Peters, J., Mead, A. and Lewis, S. (1999). TiPS receptor and ion channel nomenclature supplement 1999. *Trends Pharmacol. Sci.* **19**, 1.

Alexander, S. P. H., Christopoulos, A., Davenport, A. P., Kelly, E., Marrion, N. V., Peters, J. A., Faccenda, E., Harding, S. D., Pawson, A. J., Sharman, J. L. et al. (2017). The concise guide to pharmacology 2017/18: G protein-coupled receptors. *Br. J. Pharmacol.* **174** Suppl. 1, S17-S129.

Allen, A. E., Storchi, R., Martial, F. P., Petersen, R. S., Montemurro, M. A., Brown, T. M. and Lucas, R. J. (2014). Melanopsin-driven light adaptation in mouse vision. *Curr. Biol.* **24**, 2481-2490.

Bailes, H. J. and Lucas, R. J. (2013). Human melanopsin forms a pigment maximally sensitive to blue light (lambdamax approximately 479 nm) supporting activation of G(q/11) and G(i/o) signalling cascades. *Proc. Biol. Sci.* **280**, 20122987.

Beaulé, C., Robinson, B., Lamont, E. W. and Amir, S. (2003). Melanopsin in the circadian timing system. *J. Mol. Neurosci.* **21**, 73-89.

Bellingham, J., Chaurasia, S. S., Melyan, Z., Liu, C., Cameron, M. A., Tarttelin, E. E., Iuvone, P. M., Hankins, M. W., Tosini, G. and Lucas, R. J. (2006). Evolution of melanopsin photoreceptors: discovery and characterization of a new melanopsin in nonmammalian vertebrates. *PLoS Biol.* **4**, e254.

Bondar, A. and Lazar, J. (2014). Dissociated GalphaGTP and Gbetagamma protein subunits are the major activated form of heterotrimeric Gi/o proteins. *J. Biol. Chem.* **289**, 1271-1281.

Brown, T. M., Tsujimura, S.-I., Allen, A. E., Wynne, J., Bedford, R., Vickery, G., Vugler, A. and Lucas, R. J. (2012). Melanopsin-based brightness discrimination in mice and humans. *Curr. Biol.* **22**, 1134-1141.

Camps, M., Hou, C., Sidiropoulos, D., Stock, J. B., Jakobs, K. H. and Gierschik, P. (1992). Stimulation of phospholipase C by guanine-nucleotide-binding protein beta gamma subunits. *Eur. J. Biochem.* **206**, 821-831.

Chen, C. L., Wang, Y., Sesaki, H. and Iijima, M. (2012). Myosin I links PIP3 signaling to remodeling of the actin cytoskeleton in chemotaxis. *Sci. Signal.* **5**, ra10.

Dubocovich, M. L. and Markowska, M. (2005). Functional MT1 and MT2 melatonin receptors in mammals. *Endocrine* **27**, 101-110.

Dubocovich, M. L., Rivera-Bermudez, M. A., Gerdin, M. J. and Masana, M. I. (2003). Molecular pharmacology, regulation and function of mammalian melatonin receptors. *Front. Biosci.* **8**, d1093-d1108.

Dyachok, O., Isakov, Y., Sågetorp, J. and Tengholm, A. (2006). Oscillations of cyclic AMP in hormone-stimulated insulin-secreting beta-cells. *Nature* **439**, 349-352.

Enezi, J., Revell, V., Brown, T., Wynne, J., Schlangen, L. and Lucas, R. (2011). A "melanopic" spectral efficiency function predicts the sensitivity of melanopsin photoreceptors to polychromatic lights. *J. Biol. Rhythms* **26**, 314-323.

Ferguson, S. S. G. and Caron, M. G. (1998). G protein-coupled receptor adaptation mechanisms. *Semin. Cell Dev. Biol.* **9**, 119-127.

Gainetdinov, R. R., Premont, R. T., Bohn, L. M., Lefkowitz, R. J. and Caron, M. G. (2004). Desensitization of G protein-coupled receptors and neuronal functions. *Annu. Rev. Neurosci.* **27**, 107-144.

Gallegos, L. L., Kunkel, M. T. and Newton, A. C. (2006). Targeting protein kinase C activity reporter to discrete intracellular regions reveals spatiotemporal differences in agonist-dependent signaling. *J. Biol. Chem.* **281**, 30947-30956.

Hankins, M. W. and Hughes, S. (2014). Vision: melanopsin as a novel irradiance detector at the heart of vision. *Curr. Biol.* **24**, R1055-R1057.

Hannila, S. S. and Filbin, M. T. (2008). The role of cyclic AMP signaling in promoting axonal regeneration after spinal cord injury. *Exp. Neurol.* **209**, 321-332.

Hemrick-Luecke, S. K., Bymaster, F. P., Evans, D. C., Wess, J. and Felder, C. C. (2002). Muscarinic agonist-mediated increases in serum corticosterone levels are abolished in M_2 muscarinic acetylcholine receptor knockout mice. *J. Pharmacol. Exp. Ther.* **303**, 99-103.

Herlitze, S., Garcia, D. E., Mackie, K., Hille, B., Scheuer, T. and Catterall, W. A. (1996). Modulation of Ca2+ channels by G-protein beta gamma subunits. *Nature* **380**, 258-262.

Hughes, S., Welsh, L., Katti, C., González-Menéndez, I., Turton, M., Halford, S., Sekaran, S., Peirson, S. N., Hankins, M. W. and Foster, R. G. (2012). Differential expression of melanopsin isoforms Opn4L and Opn4S during postnatal development of the mouse retina. *PLoS ONE* **7**, e34531.

Hughes, S., Jagannath, A., Rodgers, J., Hankins, M. W., Peirson, S. N. and Foster, R. G. (2016). Signalling by melanopsin (OPN4) expressing photosensitive retinal ganglion cells. *Eye (Lond)* **30**, 247-254.

Ikeda, S. R. (1996). Voltage-dependent modulation of N-type calcium channels by G-protein beta gamma subunits. *Nature* **380**, 255-258.

Itoh, Y., Cai, K. and Khorana, H. G. (2001). Mapping of contact sites in complex formation between light-activated rhodopsin and transducin by covalent crosslinking: use of a chemically preactivated reagent. *Proc. Natl. Acad. Sci. USA* **98**, 4883-4887.

Kamp, T. J. and Hell, J. W. (2000). Regulation of cardiac L-type calcium channels by protein kinase A and protein kinase C. *Circ. Res.* **87**, 1095-1102.

Karunarathne, W. K. A., Giri, L., Patel, A. K., Venkatesh, K. V. and Gautam, N. (2013). Optical control demonstrates switch-like PIP3 dynamics underlying the initiation of immune cell migration. *Proc. Natl. Acad. Sci. USA* **110**, E1575-E1583.

Katoh, K. and Standley, D. M. (2013). MAFFT multiple sequence alignment software version 7: improvements in performance and usability. *Mol. Biol. Evol.* **30**, 772-780.

Katoh, K., Misawa, K., Kuma, K. and Miyata, T. (2002). MAFFT: a novel method for rapid multiple sequence alignment based on fast Fourier transform. *Nucleic Acids Res.* **30**, 3059-3066.

Kawano, T., Chen, L., Watanabe, S. Y., Yamauchi, J., Kaziro, Y., Nakajima, Y., Nakajima, S. and Itoh, H. (1999). Importance of the G protein gamma subunit in activating G protein-coupled inward rectifier K(+) channels. *FEBS Lett.* **463**, 355-359.

Kolsch, V., Charest, P. G. and Firtel, R. A. (2008). The regulation of cell motility and chemotaxis by phospholipid signaling. *J. Cell Sci.* **121**, 551-559.

Koyanagi, M., Takano, K., Tsukamoto, H., Ohtsu, K., Tokunaga, F. and Terakita, A. (2008). Jellyfish vision starts with cAMP signaling mediated by opsin-G(s) cascade. *Proc. Natl. Acad. Sci. USA* **105**, 15576-15580.

Lehmann, D. M., Seneviratne, A. M. P. B. and Smrcka, A. V. (2008). Small molecule disruption of G protein βγ subunit signaling inhibits neutrophil chemotaxis and inflammation. *Mol. Pharmacol.* **73**, 410-418.

Li, S., Yang, C., Zhang, L., Gao, X., Wang, X., Liu, W., Wang, Y., Jiang, S., Wong, Y. H., Zhang, Y. et al. (2016). Promoting axon regeneration in the adult CNS by modulation of the melanopsin/GPCR signaling. *Proc. Natl. Acad. Sci. USA* **113**, 1937-1942.

Masseck, O. A., Spoida, K., Dalkara, D., Maejima, T., Rubelowski, J. M., Wallhorn, L., Deneris, E. S. and Herlitze, S. (2014). Vertebrate cone opsins enable sustained and highly sensitive rapid control of Gi/o signaling in anxiety circuitry. *Neuron* **81**, 1263-1273.

Mayeenuddin, L. H., McIntire, W. E. and Garrison, J. C. (2006). Differential sensitivity of P-Rex1 to isoforms of G protein betagamma dimers. *J. Biol. Chem.* **281**, 1913-1920.
Nakajima, Y., Nakajima, S. and Kozasa, T. (1996). Activation of G protein-coupled inward rectifier K+ channels in brain neurons requires association of G protein beta gamma subunits with cell membrane. *FEBS Lett.* **390**, 217-220.
Niu, J., Profirovic, J., Pan, H., Vaiskunaite, R. and Voyno-Yasenetskaya, T. (2003). G Protein betagamma subunits stimulate p114RhoGEF, a guanine nucleotide exchange factor for RhoA and Rac1: regulation of cell shape and reactive oxygen species production. *Circ. Res.* **93**, 848-856.
Offermanns, S., Wieland, T., Homann, D., Sandmann, J., Bombien, E., Spicher, K., Schultz, G. and Jakobs, K. H. (1994). Transfected muscarinic acetylcholine receptors selectively couple to Gi-type G proteins and Gq/11. *Mol. Pharmacol.* **45**, 890-898.
Panda, S., Provencio, I., Tu, D. C., Pires, S. S., Rollag, M. D., Castrucci, A. M., Pletcher, M. T., Sato, T. K., Wiltshire, T., Andahazy, M. et al. (2003). Melanopsin is required for non-image-forming photic responses in blind mice. *Science* **301**, 525-527.
Park, D., Jhon, D. Y., Lee, C. W., Lee, K. H. and Rhee, S. G. (1993). Activation of phospholipase C isozymes by G protein beta gamma subunits. *J. Biol. Chem.* **268**, 4573-4576.
Pilorz, V., Tam, S. K. E., Hughes, S., Pothecary, C. A., Jagannath, A., Hankins, M. W., Bannerman, D. M., Lightman, S. L., Vyazovskiy, V. V., Nolan, P. M. et al. (2016). Melanopsin regulates both sleep-promoting and arousal-promoting responses to light. *PLoS Biol.* **14**, e1002482.
Pires, S. S., Shand, J., Bellingham, J., Arrese, C., Turton, M., Peirson, S., Foster, R. G. and Halford, S. (2007). Isolation and characterization of melanopsin (Opn4) from the Australian marsupial Sminthopsis crassicaudata (fat-tailed dunnart). *Proc. Biol. Sci.* **274**, 2791-2799.
Pires, S. S., Hughes, S., Turton, M., Melyan, Z., Peirson, S. N., Zheng, L., Kosmaoglou, M., Bellingham, J., Cheetham, M. E., Lucas, R. J. et al. (2009). Differential expression of two distinct functional isoforms of melanopsin (Opn4) in the mammalian retina. *J. Neurosci.* **29**, 12332-12342.
Pitcher, J. A., Inglese, J., Higgins, J. B., Arriza, J. L., Casey, P. J., Kim, C., Benovic, J. L., Kwatra, M. M., Caron, M. G. and Lefkowitz, R. J. (1992). Role of beta gamma subunits of G proteins in targeting the beta-adrenergic receptor kinase to membrane-bound receptors. *Science* **257**, 1264-1267.
Raible, F., Tessmar-Raible, K., Arboleda, E., Kaller, T., Bork, P., Arendt, D. and Arnone, M. I. (2006). Opsins and clusters of sensory G-protein-coupled receptors in the sea urchin genome. *Dev. Biol.* **300**, 461-475.
Ribeiro-Neto, F. A. and Rodbell, M. (1989). Pertussis toxin induces structural changes in G alpha proteins independently of ADP-ribosylation. *Proc. Natl. Acad. Sci. USA* **86**, 2577-2581.
Senarath, K., Ratnayake, K., Siripurapu, P., Payton, J. L. and Karunarathne, A. (2016). Reversible G protein betagamma9 distribution-based assay reveals molecular underpinnings in subcellular, single-cell, and multicellular GPCR and G protein activity. *Anal. Chem.* **88**, 11450-11459.
Senarath, K., Payton, J. L., Kankanamge, D., Siripurapu, P., Tennakoon, M. and Karunarathne, A. (2018). Ggamma identity dictates efficacy of Gbetagamma signaling and macrophage migration. *J. Biol. Chem.* **293**, 2974-2989.
Siripurapu, P., Kankanamge, D., Ratnayake, K., Senarath, K. and Karunarathne, A. (2017). Two independent but synchronized Gbetagamma subunit-controlled pathways are essential for trailing-edge retraction during macrophage migration. *J. Biol. Chem.* **292**, 17482-17495.
Smrcka, A. V. and Sternweis, P. C. (1993). Regulation of purified subtypes of phosphatidylinositol-specific phospholipase C beta by G protein alpha and beta gamma subunits. *J. Biol. Chem.* **268**, 9667-9674.
Spencer, T. and Filbin, M. T. (2004). A role for cAMP in regeneration of the adult mammalian CNS. *J. Anat.* **204**, 49-55.
Sunahara, R. K. and Taussig, R. (2002). Isoforms of mammalian adenylyl cyclase: multiplicities of signaling. *Mol. Interv.* **2**, 168-184.
Takasaki, J., Saito, T., Taniguchi, M., Kawasaki, T., Moritani, Y., Hayashi, K. and Kobori, M. (2004). A novel Galphaq/11-selective inhibitor. *J. Biol. Chem.* **279**, 47438-47445.
Tang, W. and Gilman, A. (1991). Type-specific regulation of adenylyl cyclase by G protein beta gamma subunits. *Science* **254**, 1500-1503.
Terakita, A. (2005). The opsins. *Genome Biol.* **6**, 213.
Terrillon, S. and Bouvier, M. (2004). Roles of G-protein-coupled receptor dimerization. *EMBO Rep.* **5**, 30-34.
Ueda, H., Nagae, R., Kozawa, M., Morishita, R., Kimura, S., Nagase, T., Ohara, O., Yoshida, S. and Asano, T. (2008). Heterotrimeric G protein betagamma subunits stimulate FLJ00018, a guanine nucleotide exchange factor for Rac1 and Cdc42. *J. Biol. Chem.* **283**, 1946-1953.
van Oosterhout, F., Fisher, S. P., van Diepen, H. C., Watson, T. S., Houben, T., VanderLeest, H. T., Thompson, S., Peirson, S. N., Foster, R. G. and Meijer, J. H. (2012). Ultraviolet light provides a major input to non-image-forming light detection in mice. *Curr. Biol.* **22**, 1397-1402.
van Unen, J., Stumpf, A. D., Schmid, B., Reinhard, N. R., Hordijk, P. L., Hoffmann, C., Gadella, T. W. J., Jr and Goedhart, J. (2016). A new generation of FRET sensors for robust measurement of Gαi1, Gαi2 and Gαi3 activation kinetics in single cells. *PLoS ONE* **11**, e0146789.
Weiner, O. D. (2002). Rac activation: P-Rex1 — a convergence point for PIP3 and Gβγ? *Curr. Biol.* **12**, R429-R431.
Wu, D., Katz, A. and Simon, M. I. (1993). Activation of phospholipase C beta 2 by the alpha and beta gamma subunits of trimeric GTP-binding protein. *Proc. Natl. Acad. Sci. USA* **90**, 5297-5301.

Supplemental materials

Figure S1

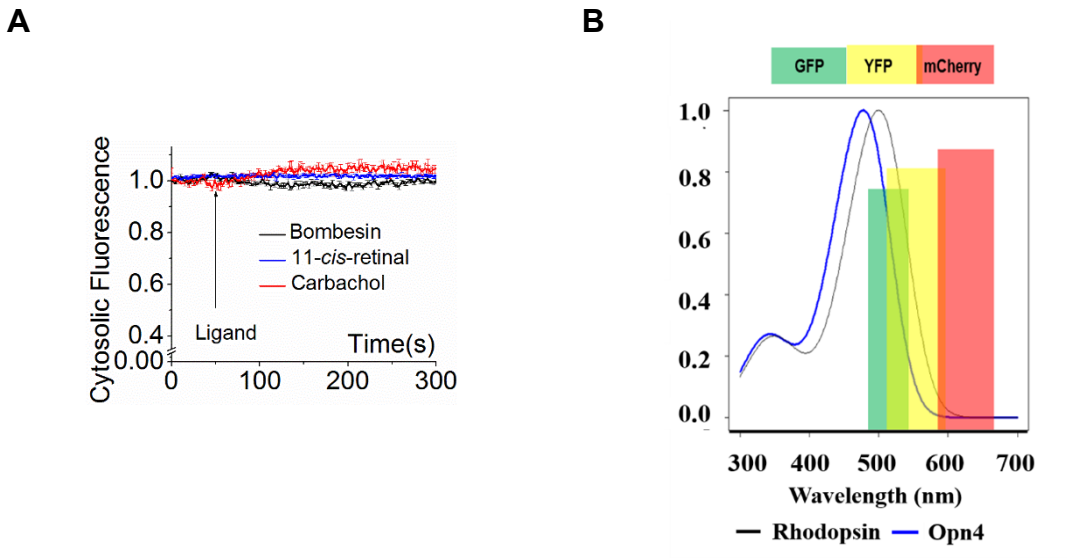

Fig. S1: (A) Without expressing corresponding receptors, the cognate ligands do not induce PIP_2 hydrolysis in HeLa cells. Cytosolic mCherry-PH fluorescence in HeLa cells after addition of Opn4, M3, and GRP receptors agonists without transfecting their respective receptors. Average curves plotted using n=10 cells from ≥3 independent experiments. Error bars: SEM. (**B) Broad absorption profile of Opn4 allow activation by blue (445nm), green (488nm), and yellow (515nm) light.** Simulated absorption spectrum of Opn4, showing that wavelengths below ~590nm can activate it.

Figure S2

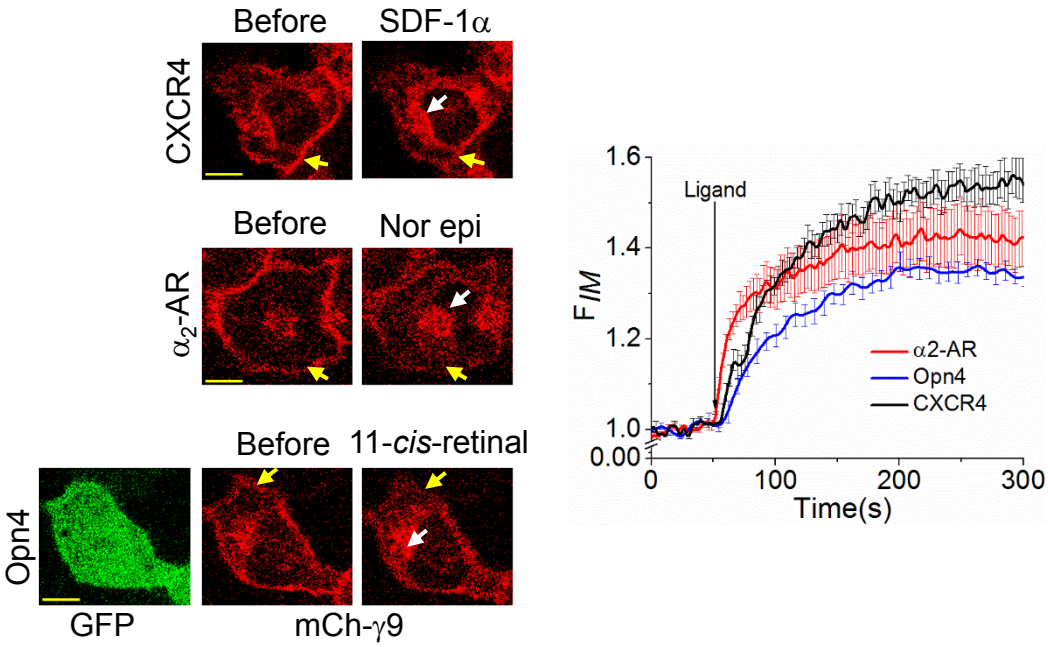

Fig. S2: Opn4 induces comparable mCherry-γ_9 translocation to G_i-coupled CXCR4 and α_2-AR. mCherry-γ_9 translocation in HeLa cells after addition of 50ng/ mL SDF-1α (top), 100μM norepinephrine (middle) to activate their respective receptors (CXCR4, α_2-AR) endogenously expressed, 50μM 11-*cis*-retinal added, imaged for mCherry and YFP to phoactivate bi-cistronic Opn4 GFP (bottom) transiently transfected in HeLa. Yellow arrows (PM), white arrows (IMs). Scale bar 10μm. Average curves plotted using n=10 cells from ≥3 independent experiments. Error bars: SEM.

Figure S3

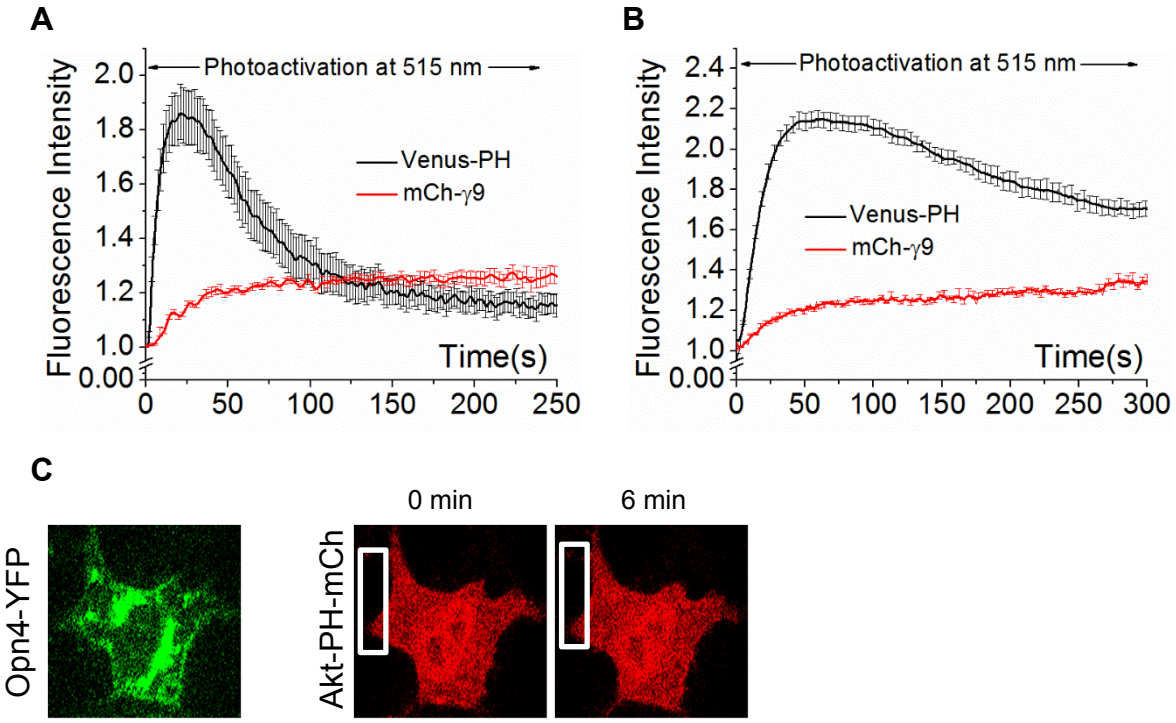

Fig. S3: (A,B) Control cells show PIP_2 hydrolysis and γ_9 translocation upon Opn4 activation. PIP_2 hydrolysis and $G\gamma_9$ translocation in HeLa cells treated with vehicle solvent used to dissolve **A**. PTx and **B.** YM-254890 after activation of Opn4. Average curves plotted using n=8 cells from ≥3 independent experiments. Error bars: SEM. **(C)** PIP3 generation in RAW264.7 in the presence of 50 μM gallein after photoactivating Opn4-YFP supplemented with 11-*cis*-retinal.

Figure S4

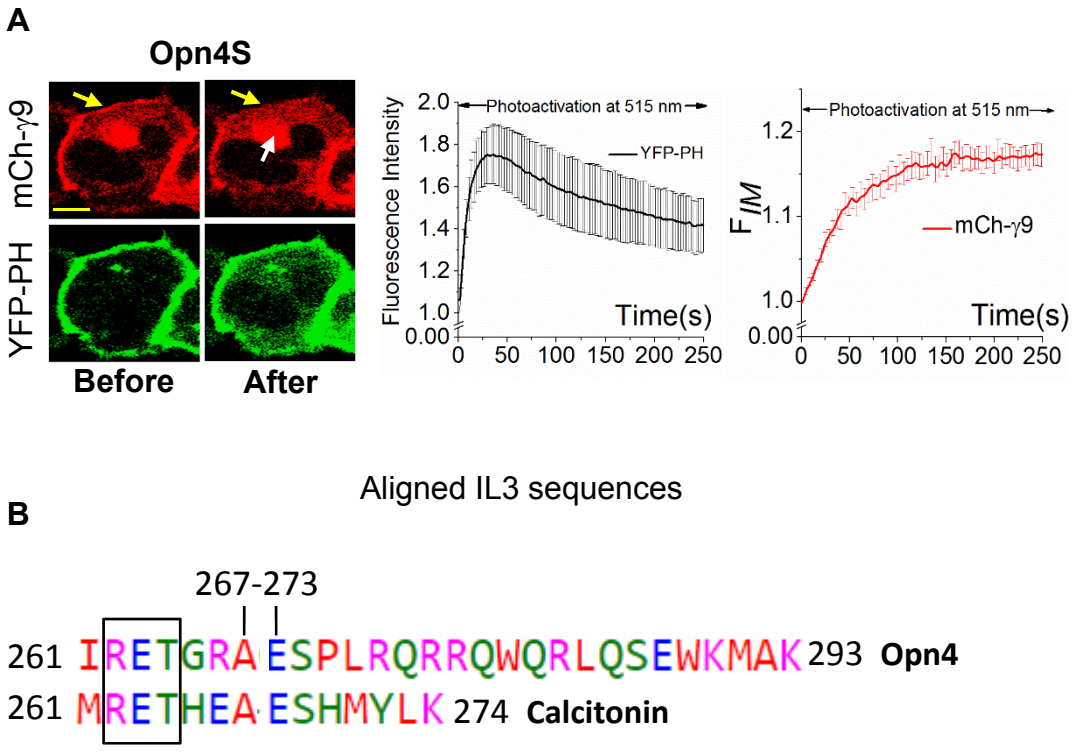

Fig. S4: (A) Similar to Opn4, Opn4S also induced PIP_2 hydrolysis and $G\gamma_9$ translocation. PIP_2 hydrolysis and $G\gamma_9$ translocation in HeLa cells after activation of Opn4S. Yellow arrows (PM), white arrows (IMs). **(B) IL3 Sequence alignments of Opn4 with G_q receptor IL3 regions that are clustered together in phylogenetic analysis.** Sequence alignment for Opn4 and G_q-coupled calcitonin receptors. Mutations in B-box resulted in a non-functional receptor. Average curves plotted using n≥10 cells from ≥3 independent experiments. Error bars: SEM.

Supplementary Movies

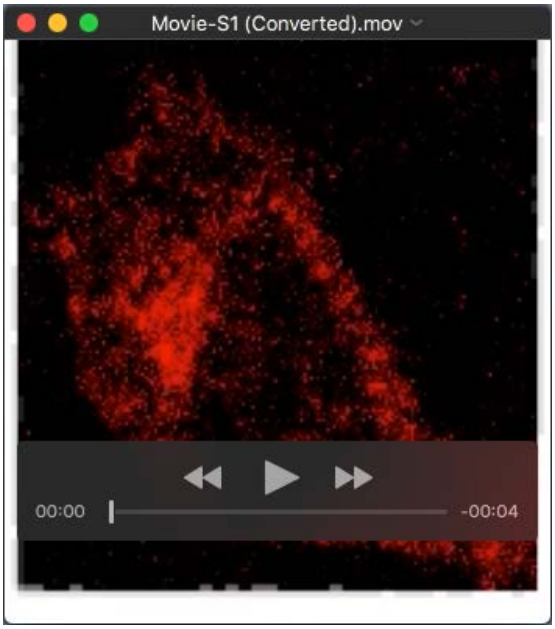

Movie-S1. A HeLa cell expressing Opn4 and PIP_2 sensor (Venus-PH) shows profound PIP_2 hydrolysis upon addition of 50 µM 11-*cis*-retinal. Scale bar 10 mm.

Movie-S2. A HeLa cell expressing Opn4 and mCh- γ_9 shows γ_9 translocation upon addition of 50 µM 11-*cis*-retinal while photoactivation at 515 nm. Scale bar 10 mm.

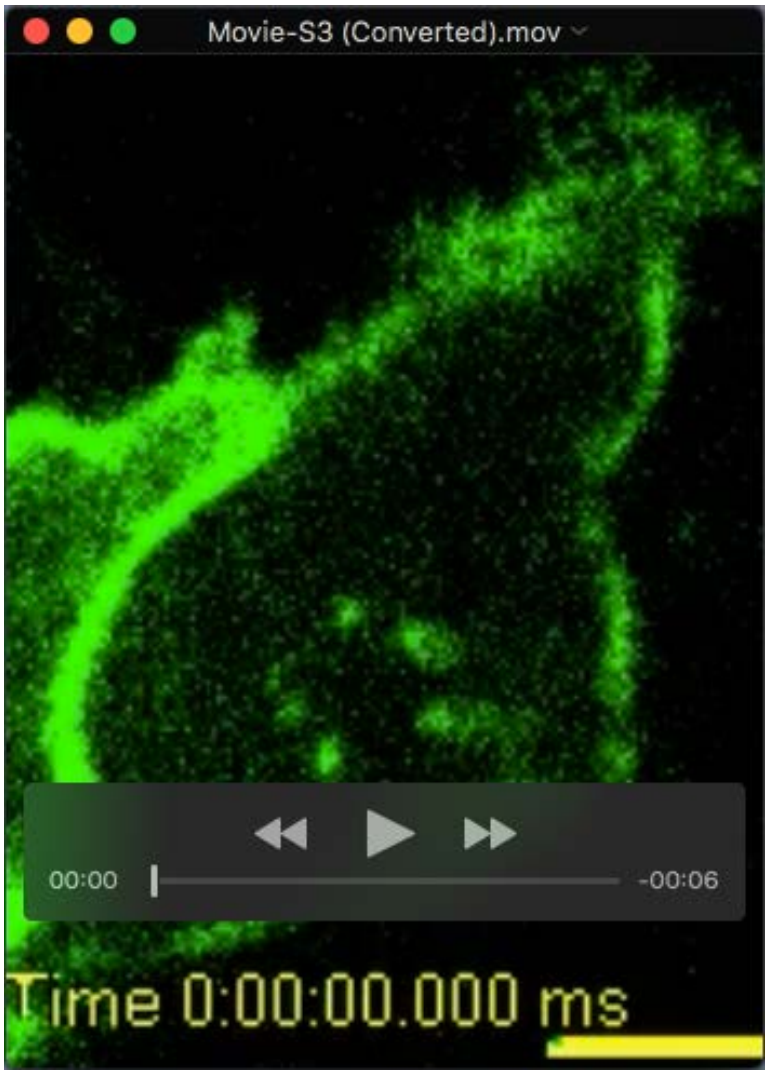

Movie-S3. A HeLa cell expressing GRPR and and PIP_2 sensor (Venus-PH) shows profound PIP_2 hydrolysis upon addition of 1 μM bombesin. Scale bar 10 mm.

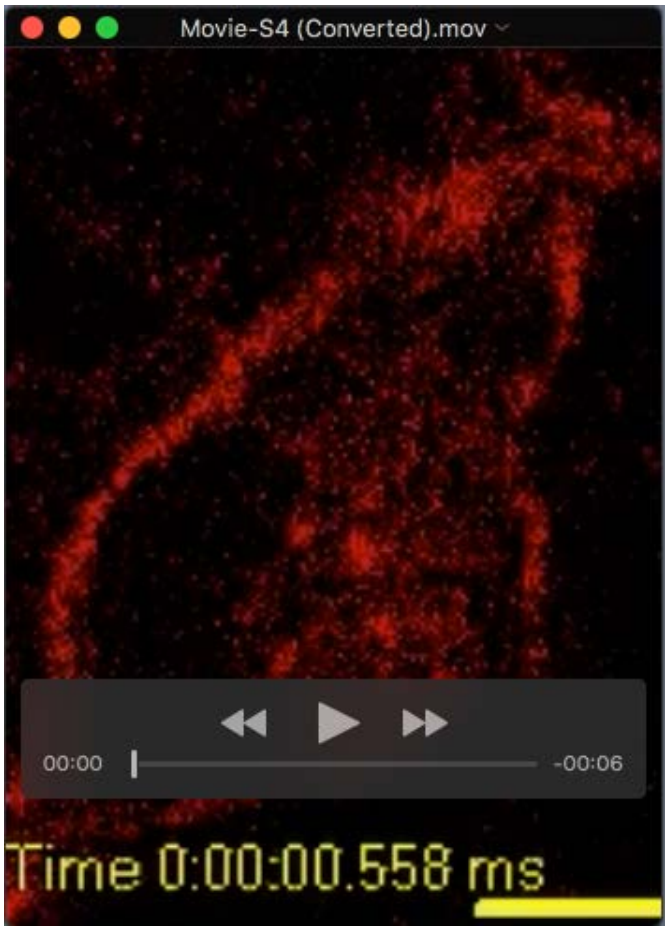

Movie-S4. A HeLa cell expressing GRPR and mCherry- γ_9 does not exhibit γ_9 translocation upon addition of 1 μM bombesin. Scale bar 10 mm.

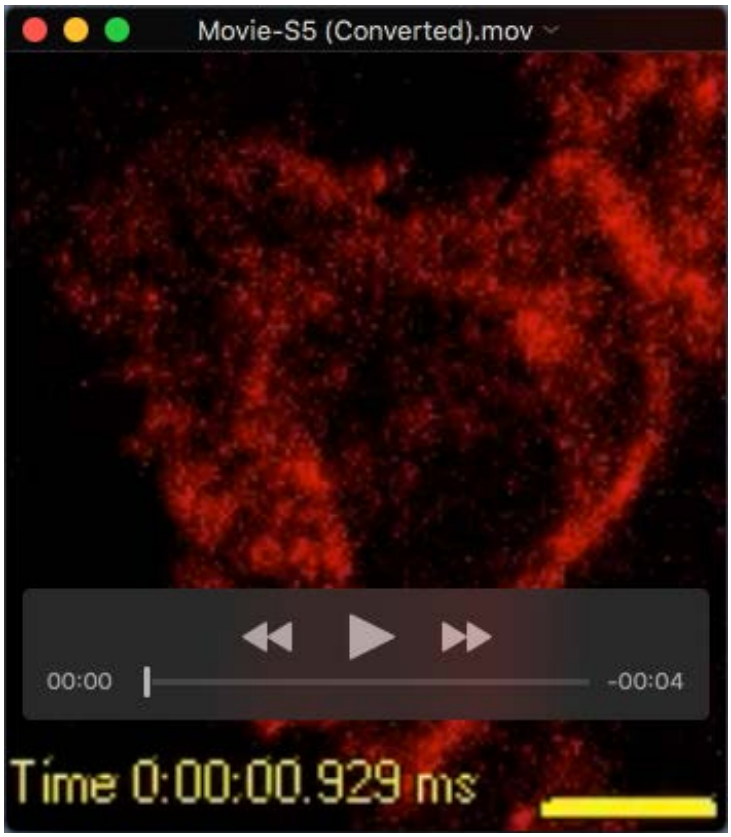

Movie-S5. A HeLa cell endogenously expressing a_2-AR and mCherry- γ_9 shows γ_9 translocation upon addition of 100 μM nor-epinephrine. Scale bar 10 mm.